EINDHOVEN UNIVERSITY OF TECHNOLOGY

# Triple axis x-ray investigations of semiconductor surface corrugations

*Citation for published version (APA):*
Darhuber, A. A., Koppensteiner, E., Straub, H., Brunthaler, G., Faschinger, W., & Bauer, G. (1994). Triple axis x-ray investigations of semiconductor surface corrugations. *Journal of Applied Physics*, *76*(12), 7816-7823. https://doi.org/10.1063/1.357915

*DOI:*
10.1063/1.357915

*Document status and date:*
Published: 01/01/1994

*Document Version:*
Publisher's PDF, also known as Version of Record (includes final page, issue and volume numbers)

***Please check the document version of this publication:***

• A submitted manuscript is the version of the article upon submission and before peer-review. There can be important differences between the submitted version and the official published version of record. People interested in the research are advised to contact the author for the final version of the publication, or visit the DOI to the publisher's website.
• The final author version and the galley proof are versions of the publication after peer review.
• The final published version features the final layout of the paper including the volume, issue and page numbers.

Link to publication

*General rights*
Copyright and moral rights for the publications made accessible in the public portal are retained by the authors and/or other copyright owners and it is a condition of accessing publications that users recognise and abide by the legal requirements associated with these rights.

• Users may download and print one copy of any publication from the public portal for the purpose of private study or research.
• You may not further distribute the material or use it for any profit-making activity or commercial gain
• You may freely distribute the URL identifying the publication in the public portal.

If the publication is distributed under the terms of Article 25fa of the Dutch Copyright Act, indicated by the "Taverne" license above, please follow below link for the End User Agreement:

www.tue.nl/taverne

*Take down policy*
If you believe that this document breaches copyright please contact us at:

openaccess@tue.nl

providing details and we will investigate your claim.

Download date: 04. Oct. 2023

# Triple axis x-ray investigations of semiconductor surface corrugations

A. A. Darhuber, E. Koppensteiner, H. Straub, G. Brunthaler, W. Faschinger, and G. Bauer
*Institut für Halbleiterphysik, J. Kepler Universität, Altenbergerstrasse 69, A-4040 Linz, Austria*

(Received 15 April 1994; accepted for publication 9 August 1994)

X-ray reciprocal space mapping around the symmetrical (004) Bragg reflection and a kinematical x-ray diffraction model were employed in order to determine the geometry and the structural perfection of surface corrugations or quantum wires. This method was used for the analysis of (001) $Cd_{1-x}Zn_xTe$ surface corrugations fabricated by holographic lithography and subsequently reactive ion etched with typical periods of 500 nm. Comparison of the measurement and simulation provides conclusive information on etching depth, wire period, wire width, and the inclination of the side walls. Furthermore, the analysis yields a parameter that contains information on side wall roughness, shape fluctuations and, in principle, the crystallographic damage caused by the reactive ion etching process. Due to the high resolution of triple axis diffractometry small strain gradients are observable in the damaged region. © *1994 American Institute of Physics.*

## I. INTRODUCTION

The investigation of the structural properties of quantum wells, multiple quantum wells (MQWs), and superlattices (SLs), i.e., of systems with a modulation of composition along the growth direction, by high resolution x-ray diffraction (HRXRD) is, nowadays, a standard method and has established itself as a routinely used post-growth analysis technique.[1–3] Recently it has been shown that double crystal x-ray diffraction (DCD) can also be used successfully for studies of laterally structured materials like corrugated surfaces,[4–6] periodic arrays of quantum wires,[7,8] and quantum boxes.[9]

In the fabrication of such structures usually holographic lithography or *e*-beam lithography with subsequent reactive ion etching is used. These fabrication methods produce not only the desired laterally periodic structures but also induce damaged layers on the surface and sidewalls of the corrugations that are very influential on the electronic and optical properties of these low dimensional quantum systems.

The structural parameters of interest are the geometrical shape of the corrugation, the corrugation width, the period, the lattice strain, and the thicknesses of the surface and sidewall damaged layers. In the first reports of HRXRD on (001) surface corrugated structures double crystal x-ray diffraction was used, i.e., $\omega$ scans for symmetric [e.g., (004)] and asymmetric (224) or (113) reflections were recorded. For the latter, in order to increase the sensitivity of the corrugations, glanzing exit conditions were used.[4]

The disadvantage of this method is the fact that in DCD the finite width of the slit (e.g., 0.1 mm) in front of the detector determines the shape of the reciprocal space probe and thus the region over which the intensity is integrated is elongated along the Ewald sphere. With the use of slits asymmetric reflections like (113) or (224) are better suited than symmetric ones, although they have a smaller structure factor than, for example, the (004) reflection. The reason for this preference is the fact that for (113) and (224) reflections the elongation of the reciprocal space probe is almost parallel to the $q_z$ direction in which the wire satellite maxima are elongated. The growth direction is assumed to be parallel to the $z$ direction in the following. The use of triple axis diffractometry (TAD), i.e., the use of analyzer crystals in between the sample and the detector significantly increases the instrument resolution[10] and thus appreciably reduces the extent of the reciprocal space probe. Two dimensional measurements of the contours of scattered intensity around reciprocal lattice points (RELPs) are possible and have been widely used in the last two years for the analysis of multilayer samples.[10]

For the structural analysis of semiconductor surface corrugations and periodic quantum wires of several III-V compounds, the technique of reciprocal space mapping has recently been applied by three groups (Gailhanou *et al.*,[11] van der Sluis *et al.*,[4] and Holy *et al.*[12]).

In this article we describe the experimental method in detail in Sec. II. The analysis of the reciprocal space maps from such corrugated systems, based on a kinematical diffraction model is presented in Sec. III. The experimental results, i.e., the reciprocal space maps around (004) reflections from corrugated $Cd_{1-x}Zn_xTe$ surfaces are described in Sec. IV. In Sec. V it is shown that apart from information on the geometrical shape, on the periodicity, and on the average strain of the corrugations, as well as the roughness of the walls, the crystallographic damage and minute strain gradients within the corrugations can be deduced from such measurements and their analysis.

Among other methods such as scanning (SEM) and transmission electron microscopy[13] (TEM), measurements of the conductance as a function of decreasing wire width,[14,15] Raman scattering,[16] and ballistic electron emission microscopy[17] (BEEM), investigations of the normalized photoluminescence versus wire width,[18] x-ray diffraction is indeed quite suitable for the characterization of the damage done by ion bombardment and of the structural quality of periodic corrugations.

## II. EXPERIMENTAL SETUP

### A. Holographic lithography and reactive ion etching

Periodic surface corrugations of $Cd_{0.96}Zn_{0.04}Te$ substrates were prepared by holographic lithography with an Ar-

 0021-8979/94/76(12)/7816/8/$6.00 © 1994 American Institute of Physics

Downloaded 14 Oct 2009 to 131.155.115.10. Redistribution subject to AIP license or copyright; see http://jap.aip.org/jap/copyright.jsp

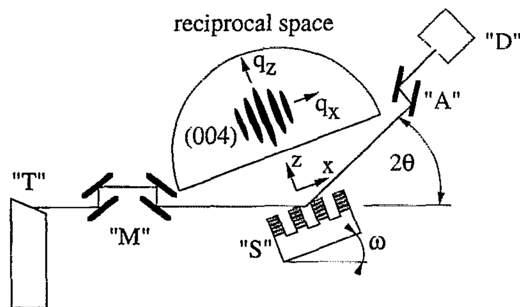


FIG. 1. Rough sketch of the experimental setup: T, M, S, A, and D denote the Cu $K\alpha_1$ x-ray tube, the four-crystal-Ge (220) monochromator, the sample, the two-crystal-Ge (220) analyzer, and the detector, respectively. Angular divergence of the beam: 12 arcsec; wavelength dispersion: $\Delta\lambda/\lambda \sim 2.3\times10^{-5}$.

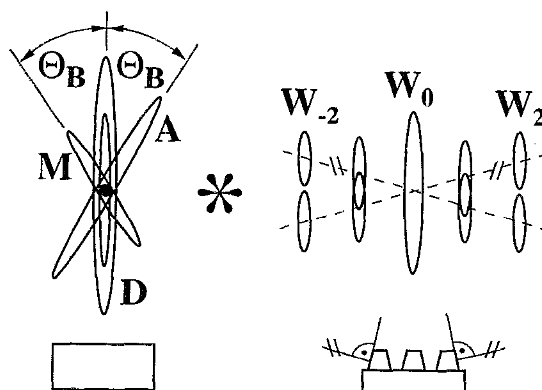


FIG. 2. If thick crystals (i.e., substrates) are corrugated, the additional features have to be taken into account: the analyzer streak A, the monochromator streak M, and the dynamical streak D (lhs). The observed diffaction pattern is a convolution (*) of the intensity distribution before etching with the pure wire diffraction pattern (satellites $W_{-2}-W_{+2}$) from the structured region.

ion laser (wavelength $\lambda=457.8$ nm). The period was nominally 500 nm. Afterwards the substrate was etched by a reactive ion etching (RIE) process. As a reactive gas a mixture of methane and hydrogen was used with a ratio $CH_4:H_2=1:6$. The molecules were ionized by a 13.56 MHz radio frequency (rf) radiation, in a parallel-plate reactor (Oxford 80 plus) with the following settings: a power of 180 W, and an acceleration voltage of 550 V. With a pressure of 25 mTorr at a flow rate of 5 sccm for $CH_4$ and 30 sccm for $H_2$ the etching rate was 30 nm min, the total etching depth was about 300 nm. After RIE the photoresist stripes were removed by exposing the samples to an oxygen plasma for 10 min with 72 W and 240 V bias. The orientation of the grating lines was [110]. The reaction products in the RIE process used are partly similar to those gases that are used in metalorganic chemical vapor deposition (MOCVD) for crystal growth of CdZnTe.

### B. X-ray measurements and analysis

A Philips MRD diffractometer with a four-crystal Ge (220) monochromator and a channel cut two crystal Ge 220 analyzer (see Fig. 1) was used. Cu $K\alpha_1$ radiation was used which leaves the Bartels type four crystal monochromator[19] with a spectral width $\Delta\lambda/\lambda=2.3\times10^{-5}$ and an angular spread of 12 arcsec. The angular resolution of the channel cut analyzer is 12 arcsec, too, which is necessary for the investigation of fine structures in a reciprocal space. Further details about the instrumentation can be found elsewhere.[20] Triple axis diffractometry benefits a lot from the use of an analyzer crystal instead of slits because of the considerably smaller reciprocal space probe and, thus, the much higher instrumental resolution. On the other hand, in TAD an artifact appears, the so-called analyzer streak for RELPs with high intensity. Its intensity is typically less than 3 counts per second (cps), which is comparable in magnitude to higher order wire satellites. For corrugated surfaces of substrates the corresponding diffraction pattern and the strong substrate RELP with its analyzer streak overlap. However, the perturbation of the measurement due to this instrument artifact is not crucial since the position of the analyzer streak is well-defined (i.e., along the Ewald sphere, intersecting the growth direction with Bragg angle $\Theta_B$).

All possible TAD artifacts are summarized in Fig. 2 (lhs), where, in addition to the analyzer streak, the so-called monochromator streak and the dynamical streak are indicated for a symmetrical diffraction. Due to the large number of reflections (for the Bartels monochromator: four) the latter streak "M" is suppressed in our case. The origin of the dynamical streak is the finite penetration depth of the x rays mainly caused by extinction. Whenever substrate and wire RELPs are separated by about 0.15°, i.e., due to a different composition or due to strain, the analyzer streak does not influence the observed pattern in the reciprocal space map at all. The analyzer streak can be completely suppressed by the use of a further analyzer crystal,[1] however, at the expense of a reduction in intensity.

## III. THEORY

In kinematical diffraction theory the x-ray amplitude $E(\mathbf{g})$ is given by

$$E(\mathbf{g}) \propto \int \rho e^{2\pi i \mathbf{g}\mathbf{r}} d^3x, \tag{1}$$

where, $\mathbf{g}$ is a vector in reciprocal space and $\rho(\mathbf{r})$ is the electron density. In our case $\rho(\mathbf{r})$ is the product of $\rho_{\text{layer}}$ and a so-called block shape (or etching) function $B(\mathbf{r})$. This function is illustrated in Fig. 3(a). $B(\mathbf{r})$ is set at zero between the wires (where no matter is situated) and equal to one for coordinates corresponding to positions $x$ within the wires. Using the convolution theorem one obtains

$$E(\mathbf{g}) \propto \int \rho_{\text{layer}} B e^{2\pi i \mathbf{g}\mathbf{r}} d^3x = \int \rho_{\text{layer}}(\mathbf{k}) B(\mathbf{k}-\mathbf{g}) d^3k. \tag{2}$$

Furthermore, one has to account for the finite wavelength dispersion[19] and the angular divergence (in the diffraction plane: 12 arcsec; perpendicular to the diffraction plane: 0.4) of the x-ray beam. Both effects decrease the area, from



Downloaded 14 Oct 2009 to 131.155.115.10. Redistribution subject to AIP license or copyright; see http://jap.aip.org/jap/copyright.jsp

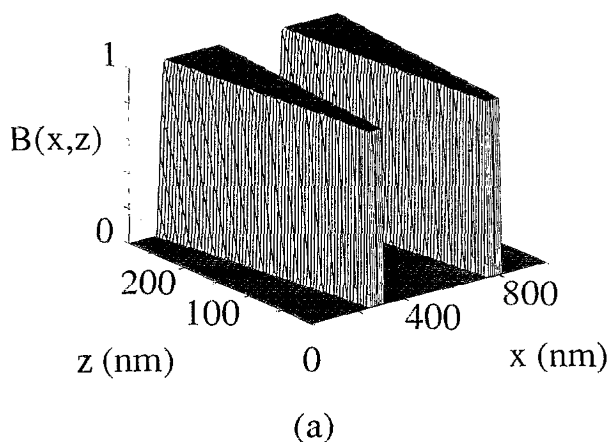


(a)

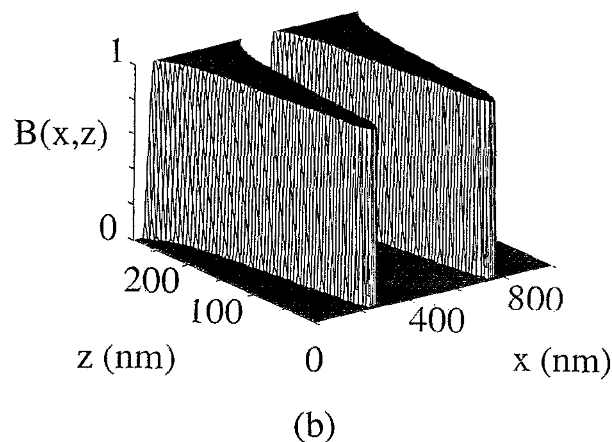


(b)

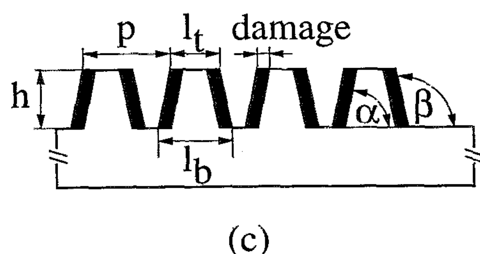


(c)

FIG. 3. (a), (b): Parts of typical blockshape functions $B(x,z)$ as used in simulation. (c): Fit parameters used in the kinematical simulations: the wire period $p$, the bottom width $l_b$, the top width $l_t$, the etching depth $h$, the inclinations of the side walls $\alpha$ and $\beta$, and the width of the outer damage cladding layer $d$.

which x rays are scattered coherently, to approximately 3 $\mu$m in the diffraction plane and to about 220 Å in the perpendicular direction. The finite coherence lengths broaden the diffraction pattern of the corrugated surfaces. These coherence lengths of 3 $\mu$m and 220 Å, respectively, follow from optical coherence theory[21] and are rigorously valid only for a homogeneously radiating and circular source. The intensity profile of the x-ray beam is strongly inhomogeneous and far from being circular. Consequently these numbers are rather orders of magnitude, but have been confirmed experimentally by measurements on nearly perfect (111) silicon single crystal wafers and will be published elsewhere.[22] For the numerical simulations, the corrugations or wires are parametrized by the following parameters:

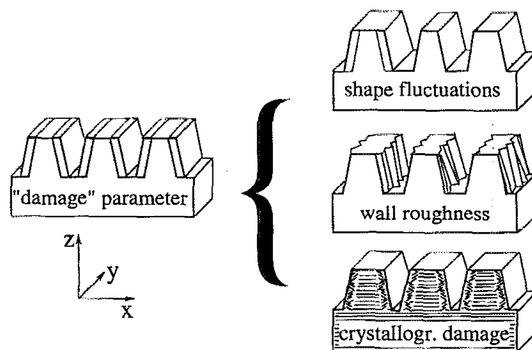


FIG. 4. Three effects contribute to the damage parameter: (i) shape fluctuations, (ii) wire wall roughness, and (iii) crystalline imperfection.

(i) the etching depth $h$,
(ii) the distance between two wires (the period length) $p$,
(iii) the bottom width $l_b$, (iv) the inclinations $(\alpha,\beta)$ of the side walls,
(iv) the amount of elastic relaxation at the top of the wire and/or the amount of a strain gradient in the sidewalls, and
(v) the damage parameter; these are defined in Fig. 3(c).

The first four parameters are accessible to scanning electron microscopy, which is routinely used for the determination of the outer geometrical shape of such corrugations. However, by employing x-ray diffraction, information on the depth and profile of the damaged regions resulting from the fabrication process is also obtained. The "damage" parameter mentioned accounts for shape fluctuations, wall roughness, and crystalline damage (see Fig. 4). However, so far the last effect has been completely overshadowed by the first two. In addition to the growth direction ($z$) defined above, we define the $y$ direction along the wires, and the $x$ direction perpendicular to both the $y$ and $z$ directions. Within the damaged region the etching function $B(x,z)$ does not change abruptly from zero to one but increases continuously within the shaded region (as shown in Fig. 4), the width of which is denoted by the damage parameter along the $x$ direction. This treatment is analogous to the calculation of the diffracted intensity from a superlattice with a transient region (i.e., intermixing) across the interfaces between the constituent materials A and B. Our model also includes the effect of strain gradients in the sidewalls or elastic relaxation at the top. The change of lattice parameters across the interface below the surface is accounted for and is shown schematically in Fig. 5. The lattice parameter change $\Delta a$ is a function of the $x$ and $z$ coordinates.

The influence of these various parameters in describing the block shape function of the wires on their diffraction patterns in the reciprocal space is shown by the simulations in Figs. 6(a)–6(f) and using Eq. (2). In Fig. 6(a) the contour plot in the reciprocal space of a wire with a rectangular cross section ($x$-$z$ plane) is shown. The distance between two wire fringes in the $q_x$ direction is proportional to the inverse of the period length $p$. The maximum corrugation period is limited to $p<1$ $\mu$m for structures of high crystalline quality because,



Downloaded 14 Oct 2009 to 131.155.115.10. Redistribution subject to AIP license or copyright; see http://jap.aip.org/jap/copyright.jsp

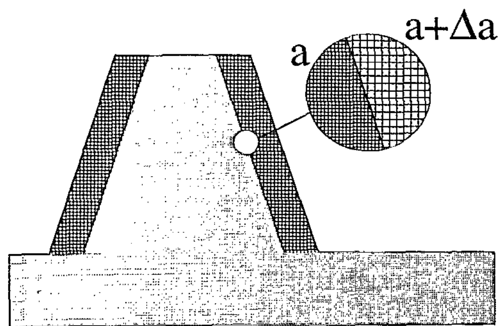


FIG. 5. Schematic representation of strain $\Delta a/a$ within the damaged region. The change in the lattice constant $\Delta a$ is not constant over the damaged region and may be caused by the implantation of reactants during the etching process.

otherwise, the wire satellites overlap in the $q_x$ direction. Both the half-width of the central maxima and the distance of the fringes accompanying them in the $q_z$ direction is proportional to the inverse of the etching depth $h$. If the height decreases by a factor of 2 [Fig. 6(b)], this half-width and the distance of the finite thickness fringes increase by a factor of 2. Simultaneously, the intensity is reduced by a factor of 4. When the period is decreased, the lateral maxima originating from the lateral wire periodicity shift towards both the left and the right of the central maximum and the whole pattern becomes more extended [Fig. 6(c)]. If the wires have inclined walls, i.e., triangular or trapezoidal cross sections, the diffraction pattern becomes a cross[3] with axes along the directions that are perpendicular to the side walls [Fig. 6(d)]. In this case the higher order satellites tend to vanish into a single omega scan (i.e., along the $q_x$ direction for a symmetric diffraction) through the symmetrical (004) intensity maximum, which would not necessarily be the case for a general oblique Bragg reflection. Because wire or corrugation cross sections are often not strictly rectangular, this simulation demonstrates the *necessity* to use *reciprocal space mapping* to get the full information on their geometrical shape.

When the cross section of the wires has a trapezoidal shape [Fig. 6(e)], the pattern is a mixture of Figs. 6(b) and 6(d). For small inclinations of the wire walls the half-widths of the lower order satellites in $q_z$ direction cannot be easily interpreted because both the etching depth as well as the inclination of the side walls affect them. However, the spacing of the thickness fringes in the $q_z$ direction is not affected at all by any inclination.

Any damage described by the corresponding damage parameter affects the envelope of the intensity contours [Fig. 6(f)]. The most pronounced effect is the remarkable decrease in intensity of the higher order satellites. For a rectangular shape of the wire cross section, this decrease occurs only along the $q_x$ direction whereas, for inclined side walls, the envelope function changes in both the $q_x$ and $q_z$ directions due to wire imperfections.

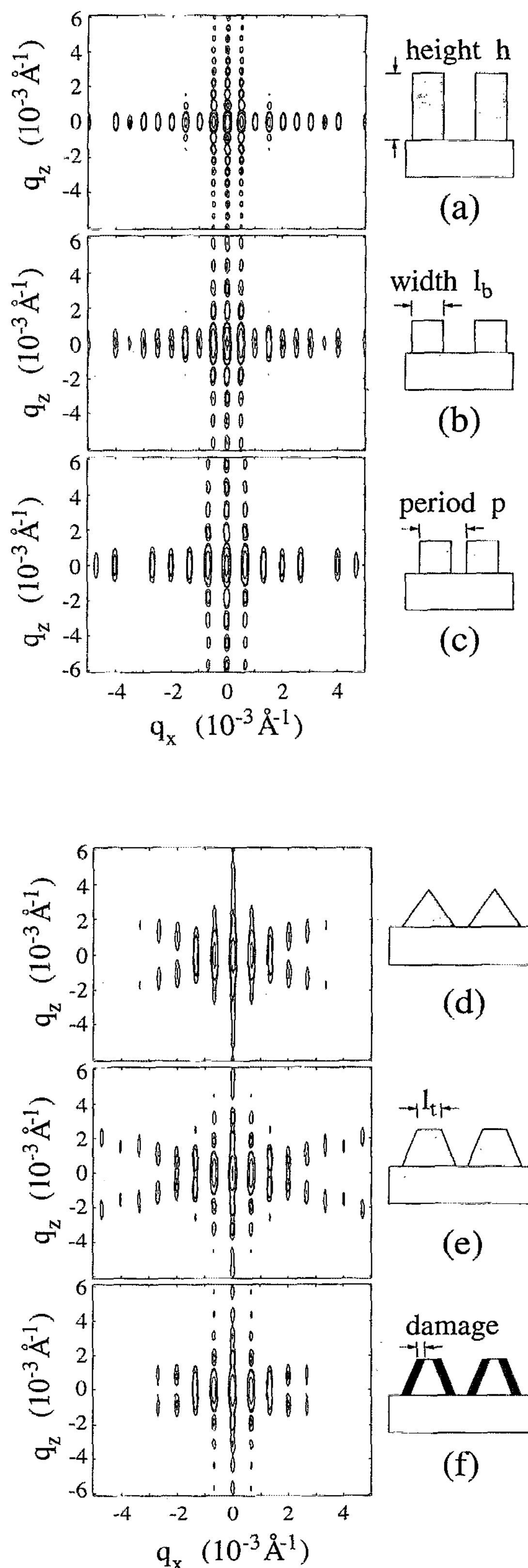


FIG. 6. Contour plots of the diffraction patterns in the reciprocal space for the following wire cross sections: (a) rectangular shape of the wires with $h$=160 nm, $l_b$=100 nm, $p$=200 nm; (b) rectangular shape with $h$=80 nm, $l_b$=100 nm, $p$=200 nm; (c) rectangular shape with $h$=80 nm, $l_b$=100 nm, $p$=150 nm; (d) triangular shape; (e) trapezoidal shape; and (f) trapezoidal shape with outer damage cladding layer.

## IV. RESULTS

In the following we compare reciprocal space maps around the (004) reflections of three lithographically defined



Downloaded 14 Oct 2009 to 131.155.115.10. Redistribution subject to AIP license or copyright; see http://jap.aip.org/jap/copyright.jsp

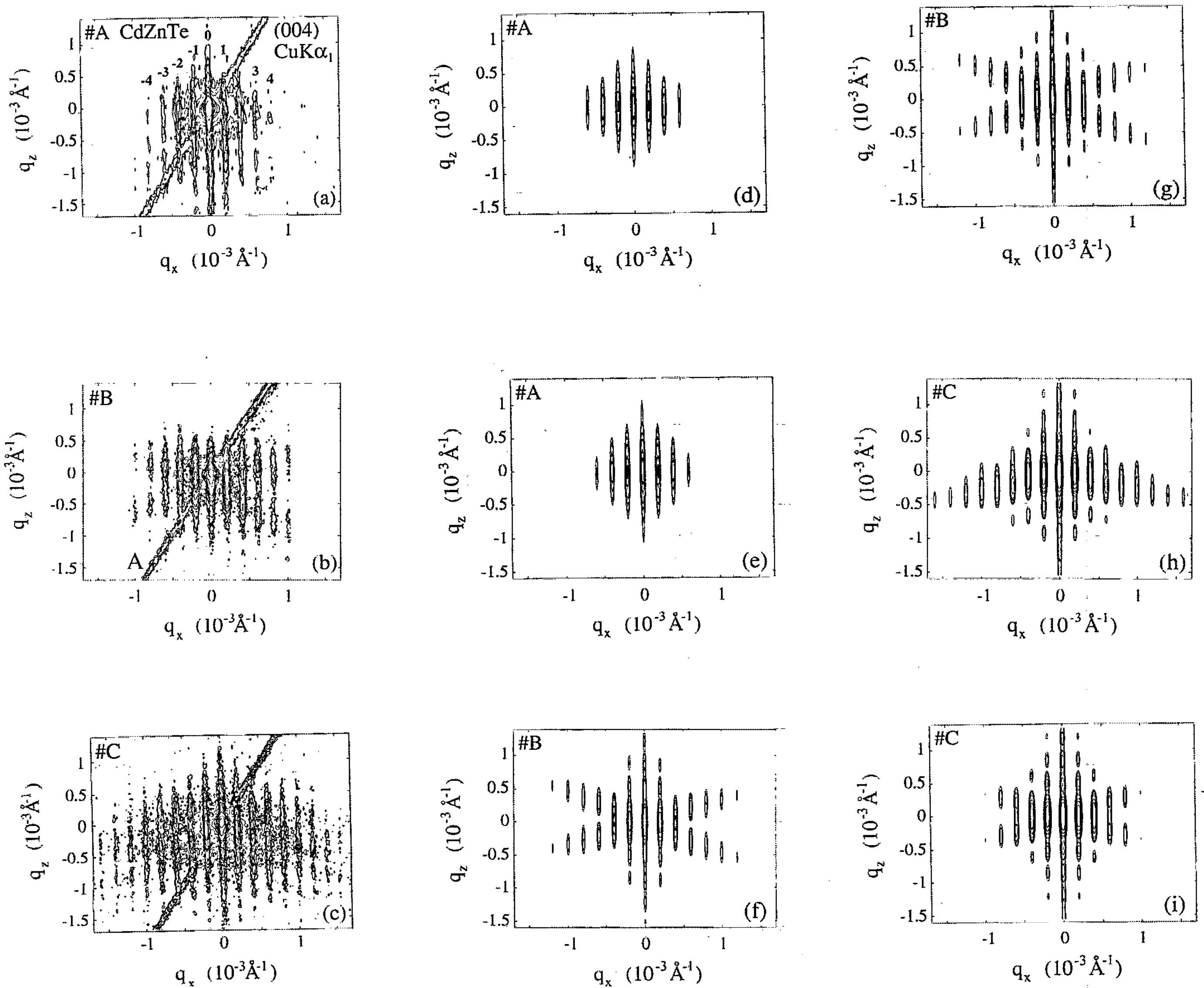


FIG. 7. Two dimensional reciprocal space maps [(a)–(c)] and simulations [(d)–(i)] of the (004) reflections in samples A–C as indicated. (d) Simulation for sample A with parameters in Table I. (e) In contrast to the simulation (d) the ridges at the top of the structure were taken into account. (f) Simulation for sample B with parameters listed in Table I. (g) In contrast to the simulation in (f) smooth corners were assumed. (h) Simulation for sample C with parameters listed in Table I. (i) Simulation of sample C without a strain gradient in the damaged region. The characteristic features in the measurement are not reproduced. Isointensity contours at 1.2, 2, 4, 7, 15, 25, 50, 100, and 500 cps.

and reactively ion etched $Cd_{1-x}Zn_xTe$ (001) substrates ($x=0.04$) with the results of simulations according to Eq. (2) (samples A, B, and C). The experimental reciprocal space maps using Cu $K\alpha_1$ radiation are shown in Figs. 7(a)–7(c). The parameters resulting from the simulations, which are shown in Figs. 7(d), 7(f), and 7(h) are summarized in Table I. In these simulations a trapezoidal shape of the wire cross section has been assumed and the notation introduced in Fig. 3 is used. The number of wire satellites observed in the (004) reciprocal space maps extends from $W_{-4}$ to $W_{+4}$ for sample A, from $W_{-5}$ to $W_{+5}$ for sample B, and from $W_{-8}$ to $W_{+8}$ for sample C. In principle, the number of observed satellites

TABLE I. Simulation parameters for shape of surface corrugations, damage, and strain in samples A to C.

| Sample | Period $p$ (nm) | Depth $h$ (nm) | Width $l_b$ (nm) | Angle $\alpha$ (°) | Angle $180-\beta$ (°) | Damage $d$ (nm) | Strain $\Delta a/a$ |
|---|---|---|---|---|---|---|---|
| A | 500±10 | 230±20 | 310±15 | 59±6 | 59±6 | 60±10 | - |
| B | 500±10 | 285±20 | 300±15 | 64±2 | 71±2 | 15±10 | - |
| C | 500±10 | 285±15 | 300±15 | 70±3 | 70±3 | 55±10 | $1.4\times10^{-4}$ |



Downloaded 14 Oct 2009 to 131.155.115.10. Redistribution subject to AIP license or copyright; see http://jap.aip.org/jap/copyright.jsp

reflects the structural perfection of the periodic corrugations in the sense that the shape fluctuations are highest in sample A. The corrugation cross sections are of a trapezoidal shape for all three samples. The cross shaped pattern of the isointensity contours is directly observable in the (004) map for sample B. This cross pattern makes it possible to determine rather precise values for the angles of inclination of the side walls. For sample A, the higher satellites have too small an intensity, and for sample C the experimental pattern is influenced by strained layer effects that will be discussed later. Furthermore, the finite height of the corrugations above the unstructured substrates causes the appearance of finite thickness fringes along the $q_z$ direction that overlap with the cross shaped pattern due to the trapezoidal shape. These finite thickness fringes are best resolved for the higher order satellites in sample C. Furthermore, from inspection of the experimental patterns in Figs. 7(a)–7(c) it follows that the trapezoidal cross section in sample A is symmetric, whereas for sample B the two inclination angles $\alpha$ and $\beta$ are somewhat different. For sample C mere inspection does not reveal any difference between $\alpha$ and $\beta$. The damage parameter $d$ varies for the three specimens from 10 to 60 nm and is highest for sample A and lowest for sample B. On the other hand, the diffraction pattern originating from sample B exhibits fewer satellites than that of sample C. Consequently, there exists no simple correlation between the number of satellites that can be observed and the width of the damaged zone if a strain gradient is present.

The simulations shown in Figs. 7(d) and 7(f) agree reasonably well with the observed isointensity contours for samples A and B. However, it turned out that the diffraction pattern is extremely sensitive to strain effects in the corrugations. In the corrugated substrates, the processing, which causes a damaged layer, is the origin of the strain. The lines connecting the intensity maxima of the wire satellites can be curved in a positive as well as in a negative $q_z$ direction, depending on the sign of the strain. For sample C, the lines connecting the higher order maxima $W_i$ ($i=-8$ to $+8$) are not parallel to the $q_x$ direction anymore, i.e., the high order satellites are either shifted downwards along the $q_z$ direction with respect to the lower order ones. This behavior follows from the comparison of the two simulations for sample C in Figs. 7(h) and 7(i). In the latter one, it is assumed that the lattice constant in the damaged cladding layer is the same as in the core of the corrugations which does not correspond to the experimental data [see Fig. 7(c)]. On the contrary, in the simulations leading to Fig. 7(h) it was assumed that there is a distinct difference $\Delta a_n$ in the lattice constant in growth direction within the outer damaged cladding layer of the corrugations. The downward shift of the higher order wire satellite maxima is connected with an increase in the lattice constant along growth direction $a_n$ in the outer damaged cladding layers.

The reason for this shift is the fact that the higher order Fourier coefficients (represented by the higher order satellite maxima) are much more affected by those parts of the corrugation that are close to the outer edges than those of the lower order ones. The latter are mainly affected by the central portion of the corrugations. Because of this, the higher order satellite maxima deviate more from the $q_z$ positions corresponding to an undistorted specimen than the lower order satellite maxima. From the simulations, it follows that one can assume that in sample C a strain as small as $\Delta a/a=1.4\times10^{-4}$ causes better agreement between the observed and calculated displacements of the outer satellites in the two dimensional diffraction pattern [compare Figs. 7(h) and 7(i)]. A possible explanation for the origin of the lattice strain in the damaged layer is perhaps the incorporation of hydrogen, carbon, or oxygen during the reactive etching process. Indeed, x-ray photoelectron spectroscopy analysis[23] on II-VI compound semiconductors etched by a $CH_4$-$H_2$ mixture revealed a high carbon contamination on the surface. Auger electron spectroscopy depth profile measurements[24] on CdS and ZnS etched with a $CH_4$-$H_2$-Ar mixture showed a penetration depth of oxygen and carbon of approximately 20 Å.

Figures 8(a) and 8(b) represent cross sections of the reciprocal space map shown in Fig. 7(a) (sample A), along the

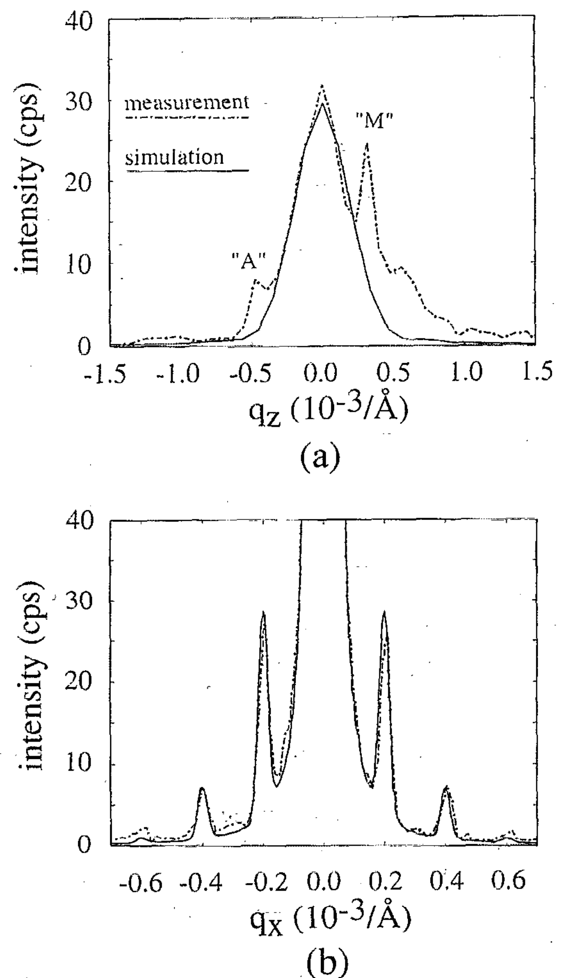


FIG. 8. (a) Cross section along the $q_z$ direction through wire satellite $W_{-1}$ of sample A including artifacts like analyzer streak A and a resonance maximum M.[11] For the simulation [see Fig. 7(d), solid line) these features have been ignored in the measurement (dash-dotted line). (b) Cross section along the $q_x$ direction through the intensity maximum in sample A. The intensity ratio of the wire satellites in the simulation (solid line) has been adjusted to that of the measurement (dash-dotted line) by an appropriate damage parameter $d$.



Downloaded 14 Oct 2009 to 131.155.115.10. Redistribution subject to AIP license or copyright; see http://jap.aip.org/jap/copyright.jsp

$q_z$ direction through the wire peak $W_{-1}$ [Fig. 8(a)] and along the $q_x$ direction [Fig. 8(b)]. The experimental trace in Fig. 8(a) shows that, in addition to the $W_{-1}$ wire peak, the FWHM of which reflects the height of the corrugation along $z$ direction, two additional peaks. The peak designated by "A" corresponds to the analyzer streak as explained in Fig. 2. Inclined under the same angle to the $q_z$ direction as the analyzer streak but on the other side (in the place of a monochromator streak, see Fig. 2), we obtained pronounced maxima, which can be understood as a consequence of the influence of the grating on the transmitted beam impinging on the substrate,[11] which does not appear in our simulation. In Fig. 8(b) the wire satellites $W_{-3}$, etc., to $W_{+3}$ are observed and agree very well with the simulation, to which a Lorentzian was added to account for the substrate peak. In the simulation, the envelope of the intensity along $q_x$ has been adjusted by a proper choice of the damage parameter.

In the following we present scanning electron micrographs for sample A for a comparison with the structural parameters listed in Table I. Not only severe fluctuations of the geometrical shape are clearly visible in Figs. 9(a) and 9(b), but also clear indications for sidewall roughness are present in the example given. However, the topmost ridges of the corrugations seen in Figs. 9(a) and 9(b) are not easily accessible to the x-ray diffraction analysis presented since these parts of the corrugations are both extremely thin [only 40–50 nm whereas the bottom width $l_b$ is 240–260 nm, see Figs. 9(a) and 9(b)] and, in addition, very likely the most damaged regions of the lateral structure. In a simulation that takes these small ridges into account [see Fig. 7(e)] the difference in the scattered intensity distribution with respect to that shown in Fig. 7(d) is negligible. Probably one would observe more pronounced differences, if higher order satellites were present. Apart from that detail, scanning electron micrographs usually are in reasonable agreement with the data obtained from the x-ray analysis. In Fig. 9(c) a SEM micrograph of sample B is shown. The sidewall roughness is much smaller than that of sample A, in agreement with the results of the simulation. The block shape function was altered according to the data from the SEM micrograph, in the sense that for the simulation shown in Fig. 7(g), smoothed corners [as in Fig. 3(b)] have been used instead of a trapezoidal cross section [Fig. 7(f)]. The differences between the two simulations are small; the satellites $W_2$ became broader in the $q_z$ direction and additional thickness fringes arise in Fig. 7(g) in comparison to Fig. 7(f). The comparison between these two pairs of simulations also exemplifies the limits of this characterization method at present.

As mentioned, the x-ray method is limited to corrugations smaller than 1 $\mu$m in period. For the investigation of quantum wires, this period does not pose a severe limitation. Quite to the contrary; narrow surface gratings are used, e.g., to enhance the luminescence intensity. Recent investigations by Gourgon *et al.*[25] on the influence of the period width of CdTe/CdZnTe wires clearly show a strong nonlinear enhancement of photoluminescence intensity if the period is decreased below 800 nm. In addition, the emission became strongly polarized along the wires for both excitation polarizations, both parallel and perpendicular to the wires. In their experiments the wire width was held constant at 80 nm.

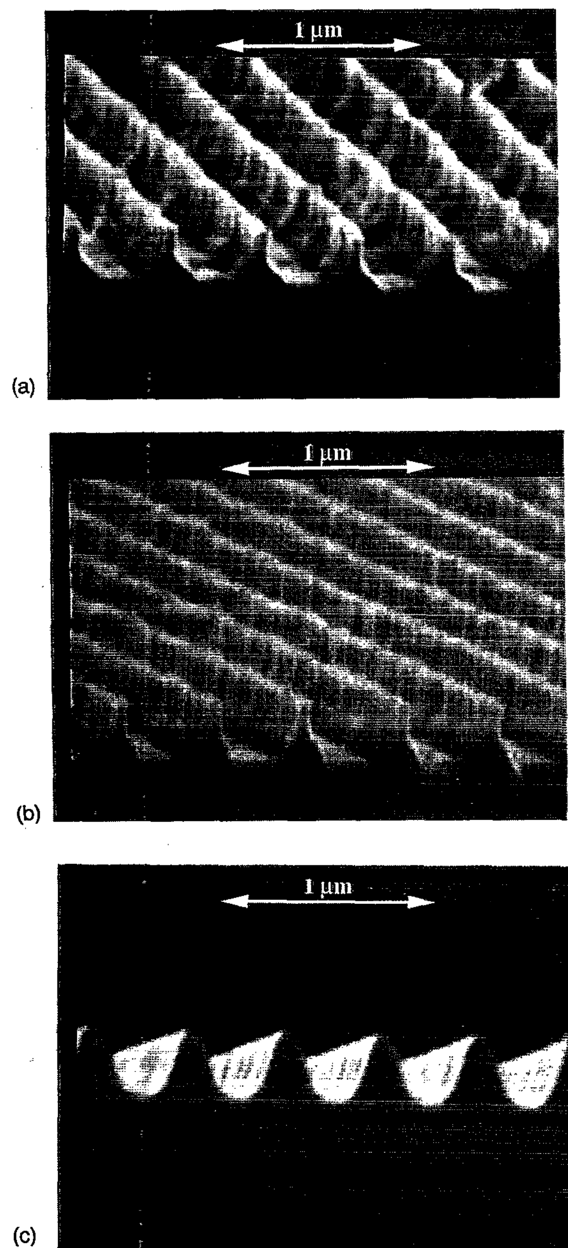


FIG. 9. SEM micrographs of samples A and B. The magnification was (a) 45 000, (b) 46 800, and (c) 47 300. Shape fluctuations are clearly visible from a comparison between (a) and (b), and even from inspection of neighboring corrugations in (b). In addition remarkable roughness of the wire sidewalls is observed, which contributes to the relatively large damage parameter found by the x-ray analysis. The sidewall roughness is much smaller for sample B, which can be clearly seen in (c). The slight asymmetry of the corrugation cross section is hardly visible on this part of the sample, but the average dimensions of the wire cross sections are in reasonable agreement with the results of the analysis method presented.

## V. CONCLUSIONS

High resolution x-ray diffraction using a triple axis instrument provides reciprocal space maps for Bragg diffractions originating from corrugated surfaces. These reciprocal space maps provide a lot of structural information not only on the geometry but also on the structural perfection of cor-



Downloaded 14 Oct 2009 to 131.155.115.10. Redistribution subject to AIP license or copyright; see http://jap.aip.org/jap/copyright.jsp

rugated semiconductor surfaces and quantum wires. Apart from the geometrical shape, the analysis of the isointensity contours of the scattered radiation yields information about the sidewall roughness, shape fluctuations, crystalline damage, and the strain status of the corrugations or wires.

The main advantages of triple axis diffractometry in this respect are the following: (i) It is nondestructive (in contrast to imaging techniques like TEM or SEM, where the samples have to be cleaved and/or thinned); and (ii) it averages over a quite large illuminated area, usually several $mm^2$. Furthermore this x-ray diffraction method is only sensitive to the crystalline part of corrugations or wires. In the latter case this determines the actual size of quantum wells in the lateral direction. There are two main limitations of this characterization method: (i) The distance between two wires must not exceed 1 $\mu$m if the crystalline quality of the etched layers is excellent; otherwise the wire satellite maxima tend to overlap completely in the $q_x$ direction and cannot be resolved anymore. (ii) The second limitation is due to the quite large lateral size of the structured area of at least 3 $mm^2$ that is necessary for collecting sufficient scattered intensity. The processing of such large areas requires a lot of time if it is done by electron beam lithography.

As far as the analysis of strain is concerned, symmetric reflections, as presented in this work, yield only information on the strain tensor component $\epsilon_{zz}$. For the analysis of the entire strain tensor (including in-plane strain effects), asymmetric reflections [e.g., (115) reflection for (001) oriented CdZnTe] have to be investigated. Also for a complete analysis of strain gradients the symmetric reflection should be complemented by an asymmetric one.

In summary, the analysis of reciprocal space maps around reciprocal lattice points resulting from Bragg diffraction of corrugated semiconductor surfaces and quantum wires yields quantitative information not only on parameters characterizing the geometrical shape but also on the presence of a damage layer and further, even on subtle lattice strain effects. The method is, of course, applicable to any corrugated crystalline semiconductor system or quantum wire.

*Note added in proof:* After submission of this manuscript we became aware of a work on GaAs corrugated surfaces studied by x-ray diffraction.[26]

## ACKNOWLEDGMENTS

This work was supported by the Bundesministerium für Wissenschaft und Forschung (Project No. GZ 601.540/1-26/92), by the Gesellschaft für Mikroelektronik (Project No. P VI/94), and by the Jubiläumsfonds der Österreichischen Nationalbank (Project Nos. 4520 and 4575).

[1] P. F. Fewster, Appl. Surf. Sci. **50**, 9 (1991).
[2] E. Koppensteiner, P. Hamberger, G. Bauer, A. Pesek, H. Kibbel, H. Presting, and E. Kasper, Appl. Phys. Lett. **62**, 1783 (1993).
[3] E. Koppensteiner, G. Bauer, V. Holy, and E. Kasper, Jpn. J. Appl. Phys. **33**, 440 (1994).
[4] P. van der Sluis, J. J. Binsma, and T. van Dongen, Appl. Phys. Lett. **62**, 3186 (1993).
[5] A. T. Macrander and S. E. G. Slusky, Appl. Phys. Lett. **56**, 443 (1990).
[6] L. Tapfer and P. Grambow, Appl. Phys. A **50**, 3 (1990).
[7] L. De Caro, P. Sciacovelli, and L. Tapfer, Appl. Phys. Lett. **64**, 34 (1994).
[8] R. Cingolani, H. Lage, L. Tapfer, H. Kalt, D. Heitmann, and K. Ploog, Phys. Rev. Lett. **67**, 891 (1991).
[9] L. Tapfer, G. C. Rocca, H. Lage, O. Brandt, D. Heitmann, and K. Ploog, Appl. Surf. Sci. **60/61**, 517 (1992).
[10] P. F. Fewster, J. Appl. Crystallogr. **24**, 178 (1991).
[11] M. Gailhanou, T. Baumbach, U. Marti, P. Silva, F. Reinhart, and M. Ilegems, Appl. Phys. Lett. **62**, 1623 (1993).
[12] V. Holy, L. Tapfer, E. Koppensteiner, G. Bauer, H. Lage, O. Brandt, and K. Ploog, Appl. Phys. Lett. **63**, 3140 (1993).
[13] R. van Roijen, C. W. T. Bulle-Lieuwma, and E. A. Montie, J. Vac. Sci. Technol. B **10**, 2188 (1992).
[14] R. Cheung, S. Thoms, I. McIntyre, C. D. W. Wilkinson, and S. P. Beaumont, J. Vac. Sci. Technol. B **6**, 1911 (1988).
[15] S. K. Murad, C. D. W. Wilkinson, P. D. Wang, W. Parkes, C. M. Sotomayor Torres, and N. Cameron, J. Vac. Sci. Technol. B **11**, 2237 (1993).
[16] D. G. Lishan, H. F. Wong, D. L. Green, E. L. Hu, and J. L. Merz, J. Vac. Sci. Technol. B **7**, 556 (1989).
[17] J. G. Couillard, A. Davies, and H. G. Craighead, J. Vac. Sci. Technol. B **10**, 3112 (1992).
[18] M. A. Foad, M. Watt, A. P. Smart, C. M. Sotomayor Torres, C. D. W. Wilkinson, W. Kuhn, H. P. Wagner, S. Bauer, H. Leiderer, and W. Gebhardt, Semicond. Sci. Technol. **6**, A115 (1991).
[19] W. J. Bartels, J. Vac. Sci. Technol. B **1**, 338 (1983).
[20] P. F. Fewster, Philips J. Res. **47**, 235 (1993).
[21] See, for example, M. Born and E. Wolf, *Principles of Optics* (Pergamon, New York, 1975).
[22] E. Koppensteiner (unpublished).
[23] M. A. Foad, C. D. W. Wilkinson, C. Dunscomb, and R. H. Williams, Appl. Phys. Lett. **60**, 2531 (1992).
[24] S. J. Pearton and F. Ren, J. Vac. Sci. Technol. B **11**, 17 (1993).
[25] C. Gourgon, B. Eriksson, Le Si Dang, H. Mariette, and C. Vieu, Proceedings of the 8th International Winterschool, Mauterndorf, Austria, 1994 (to be published in Semicond. Sci. Technology).
[26] M. Tolan, W. Press, F. Brinkop, and J. P. Kotthaus, J. Appl. Phys. **75**, 7761 (1994).



Downloaded 14 Oct 2009 to 131.155.115.10. Redistribution subject to AIP license or copyright; see http://jap.aip.org/jap/copyright.jsp